Steering, splitting, and cloning of an optical beam in a coherently driven Raman gain system

Onkar N. Verma* and Tarak N. Dey†
Department of Physics, Indian Institute of Technology Guwahati, Guwahati 781 039, Assam, India
(Received 22 September 2014; published 12 January 2015)

We propose an all-optical antiwaveguide mechanism for steering, splitting, and cloning of an optical beam without diffraction. We use a spatially inhomogeneous pump beam to create an antiwaveguide structure in a Doppler broadened $\mathcal{N}$-type four-level Raman gain medium for a copropagating weak probe beam. We show that a transverse modulated index of refraction and gain due to the spatially dependent pump beam hold the keys to steering, splitting, and cloning of an optical beam. We have also shown that an additional control field permits the propagation of an optical beam through an otherwise gain medium without diffraction and instability. We further discuss how finesse of the cloned images can be increased by changing the detuning of the control field. We arrive at similar results by using homogeneously broadened gain media at higher density.

DOI: 10.1103/PhysRevA.91.013820 PACS number(s): 42.50.Gy, 32.80.Qk, 42.65.−k

I. INTRODUCTION

Optical beam guiding, deflection, and cloning have attracted a great deal of attention due to their tremendous applications in optical imaging, optical switching, optical lithography, laser machining, and free-space communication technologies. The guiding and steering of an optical beam are made possible by virtue of a refractive index of the medium. Several techniques such as mechanical [1,2], thermal [3], electrical [4], acousto-optical [5], and all optical [6–9] have been proposed to control the refractive index for beam deflection. However, all-optical methods have been paid much effort owing to many striking features such as high speed, efficiency, and quick nonlinear response time.

The nonlinear optical interactions between light and matter create a new avenue to control beam propagation dynamics through a medium. This is feasible as the absorptive and dispersive properties of the medium can be modified by the strength of the interactions. Such manipulation of dispersion and absorption leads to many novel phenomena including electromagnetically induced transparency (EIT) [10,11], coherent population trapping [12], saturated absorption techniques [13,14], and lasing without inversion [15]. The sharp refractive index change near the center of the transparency window for the EIT medium is the key concept for beam deflection [16,17]. The ability to control light deflection is also possible by use of a transverse magnetic field through an atomic medium [18–20]. Further, a suitable spatially dependent control field can be used to modulate the refractive index along the transverse direction. This spatially modulated refractive index generates several effects such as induced focusing [21–25], waveguiding [26–29], and antiwaveguiding [30].

Most of the EIT-based schemes for producing beam deflection and guiding have low transmission due to the presence of medium absorption [16,17]. Therefore, finding an alternative medium which displays gain with the desired variation of refractive index is a challenging task. In this context, active Raman gain (ARG) media have attracted a lot of attention [31]. Recently Zhu *et al.* [32] have theoretically studied the beam deflection in an ARG medium. They have used a spatially inhomogeneous pump beam to deflect a weak probe beam. They have found that the deflection angle is increased by an order of magnitude as compared to the EIT medium. Nonetheless the probe field experiences a large amount of gain during the propagation through a Λ-type ARG medium [31,32]. This large gain makes the probe beam propagation unstable and thus limits the practical application [33–35]. Moreover, the input spot sizes for individual Gaussian profiles of pump and probe beams are equal to 1.4 cm and 1 mm, respectively. Hence, the diffraction spreading of such beams is not relevant since Rayleigh length is much larger than the length of the medium. Focusing laser beams into smaller spots [36] and increasing the spatial resolution of arbitrary images [37] is a fundamental problem in all-optical image processing [38,39]. Distortion and absorption hold the fundamental limitation for the creation, detection, or propagation of small images. This limitation affects the applications such as efficient transfer and conversion of small images [40–43], steering [44,45], or optical manipulation of light beams [46]. Here we address these issues by considering the propagation of diffraction-limited beams and arbitrary images through a controllable ARG medium.

In this paper we exploit an antiwaveguide mechanism [30] to show beam steering, splitting, and cloning of arbitrary images in inhomogeneously as well as homogeneously broadened media. To facilitate these processes, we use a spatially inhomogeneous pump beam to write an antiwaveguide inside the medium for a copropagating probe beam. At a two-photon Raman detuning condition, the refractive index and gain of the probe susceptibility are high at the peak of the Gaussian pump beam whereas at wings both are very small. The high refractive index together with gain allow us to deflect the probe beam when it is launched at the wings of the pump beam. The control field parameters such as detuning and intensity can be used to control the transmission intensity and width of the deflected probe beam for an inhomogeneously broadened medium (low density) and for a homogeneously broadened medium (high density), respectively. Next, we reveal splitting of a single super-Gaussian probe beam into two Gaussian beams by use of a two-peak pump beam structure for both broadening systems. The bright (cladding) and dark (core) regions of the pump field profile induce a high (cladding) and low (core)

*onkar@iitg.ernet.in
†tarak.dey@iitg.ernet.in

refractive index of the probe field which lead to formation of antiwaveguide structures inside inhomogeneously (low density) and homogeneously (high density) broadened media. More specifically, the super-Gaussian probe beam guided out from the core. The diffraction-limited probe beam gets focus into the cladding due to the annular profile of the refractive index. We also observe that the transmitted probe beam gets the shape of the pump beam with twice the initial finesse of the pump beam. Further, we demonstrate the cloning of a doughnut-shaped pump beam structure onto the probe beam. Our numerical simulation shows that the cloned probe has a controllable gain with high finesse. Furthermore, our scheme can be employed for cloning arbitrary pump images to the probe beam even if the pump images are severely distorted by diffraction. We find that an inhomogeneously broadened medium is more efficient for steering, splitting, and cloning of an optical beam in the low atomic density regime. A homogeneously broadened medium performs better in the high-density regime. Our findings can greatly improve the device performance on beam steering, splitting, and image cloning without diffraction.

The paper is organized as follows. In the next section, we introduce the physical model and basic equations of motion for a four-level system. In Sec. III, an approximate expression for a linear susceptibility of a weak probe field is derived using the perturbative approach. We include the thermal motion of the atoms by averaging the susceptibility over Maxwell-Boltzmann velocity distribution. In Sec. IV, we describe the beam propagation equations for the evolution of both pump and probe fields under paraxial approximations. In Sec. V, we discuss our results based on numerical simulation. We first explain the spatially dependent susceptibility for different shapes of the pump beam and advantage of a uniform control beam for both inhomogeneously as well as homogeneously broadened media. We then perform numerical integration of the beam propagation equations in order to demonstrate steering, splitting, and cloning of an optical beam for both systems. Obtained results are summarized in the final section.

II. PHYSICAL MODEL AND BASIC EQUATIONS

The schematic of the system under consideration for the generation of steering, splitting, and cloning of an optical beam is illustrated in Fig. 1(a), where three copropagating fields interact within the inhomogeneously broadened medium. The electrical dipole allowed transitions $|1\rangle \leftrightarrow |3\rangle, |3\rangle \leftrightarrow |2\rangle$, and $|2\rangle \leftrightarrow |4\rangle$ form a four-level $\mathcal{N}$-type atomic system as shown in Fig. 1(b). The transitions $|1\rangle \leftrightarrow |2\rangle, |3\rangle \leftrightarrow |4\rangle$ and $|1\rangle \leftrightarrow |4\rangle$ are generally forbidden electric dipole transitions. The atomic transitions $|3\rangle \leftrightarrow |1\rangle, |3\rangle \leftrightarrow |2\rangle$, and $|4\rangle \leftrightarrow |2\rangle$ are driven by a pump field with frequency ω_1, a weak probe field with frequency ω_2, and a control field with frequency ω_3, respectively. This generic level configuration can be found for example in energy levels of ^{87}Rb which contain ground levels

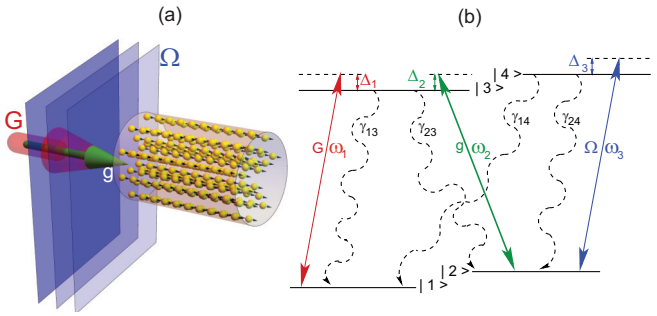

FIG. 1. (Color online) (a) Schematic illustration to produce steering, splitting, and cloning of the optical beam. The beam shaped pump, probe, and a plane-wave control fields are copropagating with the thermal ^{87}Rb atoms. (b) Energy-level diagram of a four-level ^{87}Rb atomic system in $\mathcal{N}$ configuration. The atomic transition $|3\rangle \leftrightarrow |1\rangle$ is coupled by a pump field of Rabi frequency G. The weak probe field of Rabi frequency g interacts with the atomic transition $|3\rangle \leftrightarrow |2\rangle$. A control field of Rabi frequency Ω connects the transition $|4\rangle \leftrightarrow |2\rangle$ to produce controllable gain of the system.

$|1\rangle = |5S_{1/2}, F = 2\rangle, |2\rangle = |5S_{1/2}, F = 3\rangle$ and excited levels $|3\rangle = |5P_{1/2}, F' = 2\rangle$ and $|4\rangle = |5P_{3/2}, F' = 4\rangle$, respectively [47,48].

We define three copropagating electric fields as follows:

$$\vec{E}_j(\vec{r},t) = \hat{e}_j \mathcal{E}_j(\vec{r}) e^{-i(\omega_j t - k_j z)} + \text{c.c.}, \tag{1}$$

where $\mathcal{E}_j(\vec{r})$ are slowly varying envelopes, $\hat{e}_j$ is the unit polarization vector, and k_j is the wave number of electric fields. The index $j \in \{1,2,3\}$ denotes the pump, probe, and control fields, respectively. Under the action of three coherent fields, the interaction Hamiltonian of the system in the dipole and rotating wave approximation is given by

$$\begin{aligned}\mathcal{H}_I/\hbar = {} & (\Delta_2 - \Delta_1 - \Delta_3)|4\rangle\langle 4| - (\Delta_1 - \Delta_2)|2\rangle\langle 2| - \Delta_1 |3\rangle\langle 3| \\ & - (g|3\rangle\langle 2| + G\,|3\rangle\langle 1| + \Omega\,|4\rangle\langle 2| + \text{H.c.}),\end{aligned} \tag{2}$$

where $\Delta_1 = \omega_1 - \omega_{31}, \Delta_2 = \omega_2 - \omega_{32}, \Delta_3 = \omega_3 - \omega_{42}$ are the single-photon detunings of the pump, probe, and control fields, respectively. The atomic transition frequencies are denoted by ω_{ij}. The Rabi frequencies of pump, probe, and control fields are defined as

$$G = \frac{\vec{d}_{13} \cdot \vec{\mathcal{E}}_1}{\hbar}, \quad g = \frac{\vec{d}_{23} \cdot \vec{\mathcal{E}}_2}{\hbar}, \quad \text{and} \quad \Omega = \frac{\vec{d}_{24} \cdot \vec{\mathcal{E}}_3}{\hbar}, \tag{3}$$

where the d_{ij} are the corresponding dipole moment matrix elements of transitions $|i\rangle \leftrightarrow |j\rangle$.

The dynamical evolution of the atomic system can be described by the density-matrix equations [37],

$$\dot{\rho} = -\frac{i}{\hbar}[\mathcal{H}_I, \rho] + \mathcal{L}\rho, \tag{4}$$

where the Liouvillian matrix $\mathcal{L}\rho$, defined in Eq. (5), describes the relaxation by radiative and nonradiative decay:

$$\mathcal{L}\rho = \begin{bmatrix} \gamma_{13}\rho_{33} + \gamma_{14}\rho_{44} & -\gamma_c \rho_{12} & -\Gamma_{13}\rho_{13} & -\Gamma_{14}\rho_{14} \\ -\gamma_c \rho_{21} & \gamma_{23}\rho_{33} + \gamma_{24}\rho_{44} & -\Gamma_{23}\rho_{23} & -\Gamma_{24}\rho_{24} \\ -\Gamma_{31}\rho_{31} & -\Gamma_{32}\rho_{32} & -(\gamma_{13} + \gamma_{23})\rho_{33} & -\Gamma_{34}\rho_{34} \\ -\Gamma_{41}\rho_{41} & -\Gamma_{42}\rho_{42} & -\Gamma_{43}\rho_{43} & -(\gamma_{14} + \gamma_{24})\rho_{44} \end{bmatrix}. \tag{5}$$

The radiative decay rates from the excited states $|3\rangle$ and $|4\rangle$ to ground states $|1\rangle$ and $|2\rangle$ are labeled by γ_{i3} and $\gamma_{i4}, i \in \{1,2\}$ and the collisions dephasing rate γ_c describes redistribution of populations between ground levels. The decay rate of the atomic coherence is defined as

$$\Gamma_{\alpha\beta} = \frac{1}{2}\left[\sum_i \gamma_{i\alpha} + \sum_i \gamma_{i\beta}\right] + \gamma_c, i \notin \{\alpha,\beta\}. \quad (6)$$

Substituting the interaction Hamiltonian of Eq. (2) and the Liouvillian matrix of Eq. (5) in the density matrix Eq. (4), the equations of motion for the four-level atomic system can be described as

$$\begin{aligned}
\dot{\rho}_{11} &= \gamma_{13}\rho_{33} + \gamma_{14}\rho_{44} + iG^*\rho_{31} - iG\rho_{13}, \\
\dot{\rho}_{22} &= \gamma_{23}\rho_{33} + \gamma_{24}\rho_{44} + ig^*\rho_{32} - ig\rho_{23} + i\Omega^*\rho_{42} - i\Omega\rho_{24}, \\
\dot{\rho}_{21} &= -[\gamma_c - i\Delta_R]\rho_{21} - iG\rho_{23} + ig^*\rho_{31} + i\Omega^*\rho_{41}, \\
\dot{\rho}_{33} &= -(\gamma_{13} + \gamma_{23})\rho_{33} + iG\rho_{13} - iG^*\rho_{31} + ig\rho_{23} - ig^*\rho_{32}, \\
\dot{\rho}_{31} &= -[\Gamma_{31} - i\Delta_1]\rho_{31} + ig\rho_{21} + iG(\rho_{11} - \rho_{33}), \\
\dot{\rho}_{32} &= -[\Gamma_{32} - i\Delta_2]\rho_{32} + iG\rho_{12} - i\Omega\rho_{34} + ig(\rho_{22} - \rho_{33}), \\
\dot{\rho}_{34} &= -[\Gamma_{34} - i(\Delta_2 - \Delta_3)]\rho_{34} + iG\rho_{14} + ig\rho_{24} - i\Omega^*\rho_{32}, \\
\dot{\rho}_{41} &= -[\Gamma_{41} - i(\Delta_R + \Delta_3)]\rho_{41} + i\Omega\rho_{21} - iG\rho_{43}, \\
\dot{\rho}_{42} &= -[\Gamma_{42} - i\Delta_3]\rho_{42} + i\Omega(\rho_{22} - \rho_{44}) - ig\rho_{43}, \quad (7)
\end{aligned}$$

together with population conservation condition $\rho_{11} + \rho_{22} + \rho_{33} + \rho_{44} = 1$ and two-photon Raman detuning $\Delta_R = \Delta_1 - \Delta_2$. In the next section, we obtain the analytical expression for the linear susceptibility of the probe field in a compact form with the assumption of equal decay rates from excited states, i.e., $\gamma_{13} = \gamma_{23} = \gamma_{14} = \gamma_{24} = \gamma/2$.

III. PROBE SUSCEPTIBILITY FOR HOT ATOMIC MEDIUM

In this section, we derive an approximate solution of linear susceptibility of the probe field in a hot atomic medium. The analytical solution of the atomic coherence ρ_{32} for the probe field can be obtained by solving the density matrix Eqs. (7) in the steady-state condition.

We assume that all atoms are prepared initially in the ground state $|1\rangle$. Due to the presence of large detuning of the strong pump and weak probe fields, most of the atoms populate at their ground state $|1\rangle$ while other states $|j\rangle (j \neq 1)$ remain empty at a later time. Hence the system turns to an ARG configuration for the probe field. Since the Raman gain process is basically a second-order process, we therefore expand the density-matrix elements to first order in the probe field g and to second order in the pump field G but all orders in the control field Ω in the weak probe field limit. The perturbation expansion of the density matrix can be expressed as

$$\begin{aligned}
\rho_{ij} = \rho_{ij}^{(0)} &+ G\rho_{ij}^{(1)} + G^*\rho_{ij}^{(2)} + g\rho_{ij}^{(3)} + g^*\rho_{ij}^{(4)} + G^2\rho_{ij}^{(5)} \\
&+ |G|^2\rho_{ij}^{(6)} + G^{*2}\rho_{ij}^{(7)} + gG\rho_{ij}^{(8)} + gG^*\rho_{ij}^{(9)} \\
&+ g^*G\rho_{ij}^{(10)} + g^*G^*\rho_{ij}^{(11)} + g|G|^2\rho_{ij}^{(12)}, \quad (8)
\end{aligned}$$

where $\rho_{ij}^{(0)}$ describes the solution in the absence of all three optical fields and $\rho_{ij}^{(k)}$ denotes the kth-order solution. Now we substitute the above expression in Eqs. (7) and equate the coefficients of g, g^*, G^n ($n \in 1,2$), and constant terms. As a result, we obtain a set of 12 coupled simultaneous linear algebraic equations to determine the expression of $\rho_{32}^{(12)}$. We use the back substitution method to solve these algebraic equations in order to derive the probe coherence ρ_{32}. The different terms in the expression of the probe coherence are given in the Appendix. The atomic coherence ρ_{32} will yield the probe susceptibility χ at frequency ω_2:

$$\chi(\Delta_2) = \frac{N|d_{32}|^2}{\hbar}\rho_{32}, \quad (9)$$

where N is the atomic density of the homogeneously broadened medium. The above analysis is valid for stationary atoms. The thermal motion of the atoms causes inhomogeneous broadening of the atomic spectra. The effects of atomic motion can be included in the susceptibility expression (9) by introducing velocity-dependent field detunings $\Delta_j(v) = \Delta_j - k_j v, j \in \{1,2,3\}$. The term $k_j v$ is the Doppler shift experienced by an atom with a velocity component v in the direction of the beam propagation of the fields. We have assumed the wave vectors of the three fields are nearly equal ($k_j \approx k$). The negative sign in the velocity-dependent field detuning $\Delta_j(v)$ indicates that the atom and field are copropagating. The susceptibility of a hot atomic vapor system needs to be averaged over the entire velocity distribution of atoms and it is given by

$$\langle\chi\rangle = \int_{-\infty}^{\infty} \chi(kv)P(kv)d(kv). \quad (10)$$

The velocity distribution of the atom is assumed to obey the Maxwell-Boltzmann distribution:

$$P(kv)d(kv) = \frac{1}{\sqrt{2\pi\mathcal{D}^2}} e^{-\frac{(kv)^2}{2\mathcal{D}^2}} d(kv). \quad (11)$$

The Doppler width $\mathcal{D}$ at temperature T is defined by

$$\mathcal{D} = \sqrt{\frac{k_B T\omega^2}{Mc^2}}, \quad (12)$$

where M is the atomic mass and k_B is the Boltzmann constant. Doppler broadening plays a crucial role to control the width of the absorption or gain window of the thermal media [49–52]. The spectral features of the window become narrower in a Doppler broadened medium as compared with the homogeneous medium. The steepness of the refractive index due to the narrowing of the resonance window can be useful in many applications such as slow light, storage of light, and high-resolution spectroscopy. Thus we include the atomic velocity effect on the beam propagation dynamics through the ARG medium by considering Doppler averaging in the susceptibility expression.

IV. BEAM PROPAGATION EQUATIONS AND BEAM PROFILES

The propagation of copropagating pump and probe fields with amplitudes $\mathcal{E}_1$ and $\mathcal{E}_2$ along the z direction is governed by Maxwell's wave equations. Under slowly varying envelope and paraxial wave approximations, the beam propagation

equations for the pump and probe field can be expressed in the following form:

$$\frac{\partial G}{\partial z} = \frac{i}{2k_1}\left(\frac{\partial^2}{\partial x^2} + \frac{\partial^2}{\partial y^2}\right) G\,, \tag{13a}$$

$$\frac{\partial g}{\partial z} = \frac{i}{2k_2}\left(\frac{\partial^2}{\partial x^2} + \frac{\partial^2}{\partial y^2}\right) g + 2i\pi k_1 \langle\chi\rangle g\,. \tag{13b}$$

The velocity-averaged susceptibility $\langle\chi\rangle$ is included only in the probe beam equation, whereas this effect is very negligible on the pump beam propagation under the weak probe field [41]. The second partial derivatives in the transverse directions (x,y) represent a paraxial diffraction. The diffraction of the beam or image is inevitable since its constituent plane-wave components acquire different phases during its propagation. The spatially dependent refractive index of the fields can be used to suppress or even reverse due to diffraction. We use a suitable spatially dependent pump field to produce a spatially dependent refractive index for the probe field. For this purpose, we choose the transverse spatial profile of the pump beam as a Laguerre-Gaussian with charge m, denoted by LGP_m. The profile of the pump beam can be written as

$$G(x,y,z) = G_0 \frac{w_0}{w_z}\left(\frac{\sqrt{2}r}{w_z}\right)^m \exp\left[\frac{ikr^2}{2R_z} - \frac{r^2}{w_z^2}\right] \times \exp\left[-i(m+1)\tan^{-1}\left(\frac{z}{z_R}\right) + im\theta\right], \tag{14}$$

where G_0 is an initial peak amplitude and m is the azimuthal index. The beam width is defined as $w_z = w_0\sqrt{1+(z/z_R)^2}$, where w_0 is the beam waist at $z=0$, and $z_R = \pi w_0^2/\lambda$ is the Rayleigh length. The radial distance from the axis of the beam is given by $r = \sqrt{x^2+y^2}$. Note that for the azimuthal index $m=0$ the Laguerre-Gaussian pump (LGP_m) beam reduces to a Gaussian pump beam (GP_0). Figure 2 shows the intensity distribution of the pump field against radial position x at different lengths of the medium. The LGP_m beam exhibits a dark spot in the center and a bright profile in the annular region. This makes the intensity profile in contrast to the GP_0 beam. It is clearly shown in Fig. 2 that diffraction induced distortion of the pump beam profile is not severe even after 5 cm of propagation. Therefore, phase modulation imposed on the probe beam due to the spatially varying pump beam is effective throughout the length of the medium. The probe beam possesses a Gaussian profile,

$$g(x,y) = g_0\, e^{-[\frac{(x-a)^2+y^2}{w_p^2}]^f}\,, \tag{15}$$

at an entry face of the medium. The initial peak amplitude and the width of the probe field are denoted by g_0 and w_p, and a is the initial location of the center of the probe beam along the x direction. We have chosen the initial intensity of the probe beam such that it gets absorbed inside the medium without pump and control fields. The integer values of f decide the input profile of the probe beam—either a Gaussian ($f=1$) or a super-Gaussian ($f>1$).

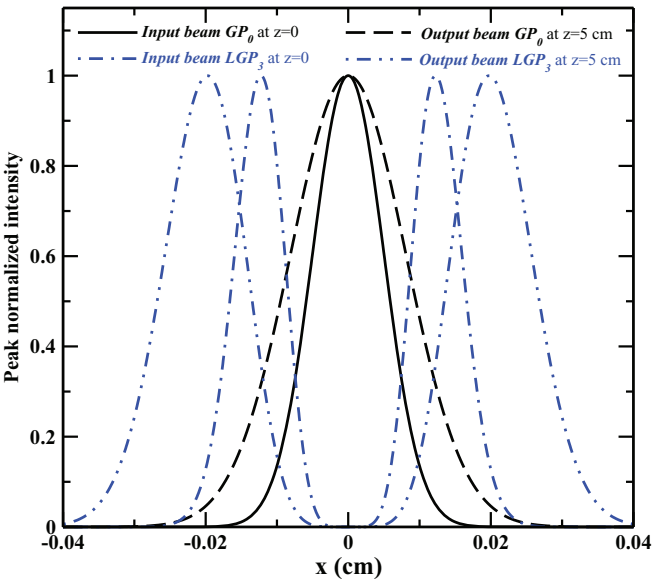

FIG. 2. (Color online) Pump intensities profile for two different shapes; namely, Gaussian (GP_0) and Laguerre-Gaussian (LGP_3) are plotted against x at the $y=0$ plane. The initial amplitude and width of the profiles are $G_0 = 2\gamma$ and $w_0 = 100\,\mu$m, respectively.

V. RESULTS AND DISCUSSIONS

A. Spatial modulation of the probe field susceptibility

In order to elucidate the effect of position dependent characteristics of the pump field on the probe beam dynamics, we first numerically explore the behavior of velocity-averaged probe susceptibility under different detuning and intensity of the control field. Figure 3 shows the spatial variation of probe dispersion and gain plotted against transverse axis x at the $y=0$ plane. Here two different transverse profiles of the pump beam, namely, Gaussian (GP_0) and Laugerre-Gaussian (LGP_3), have been used. We begin with the Gaussian pump beam and study the usefulness of uniform control field Ω on the spatially modulated probe susceptibility. The position dependent refractive index of the probe is zero under the two-photon Raman condition whereas the spatial gain profile of the probe field takes the shape of the pump beam profile in the absence of a control field ($\Omega=0$) as shown by the black dotted line in Fig. 3. The spatially dependent pump structure generates a probe gain profile which is one of the key components in realizing the deflection of the probe beam if it is off-centered with respect to the pump beam. In the absence of the control field ($\Omega=0$), the gain profile of the probe field is 15 times larger than in the case of control field $\Omega=\gamma$. This large gain can create modulation instability of the system [33–35]. Therefore a controllable gain of the medium is required to avoid the modulation instability. It is clear from Fig. 3 that the position dependent probe gain can be substantially suppressed by a uniform control field with $\Omega(x,y)=\gamma$. This restricted probe gain is accompanied by a Gaussian shaped spatial refractive index. The gradient of the refractive index is dependent on the sign of the control field detuning. At red control field detuning, the slope of the spatial refractive index attains its maximum at the line center and decreases gradually toward the wings. Hence, a convex lens

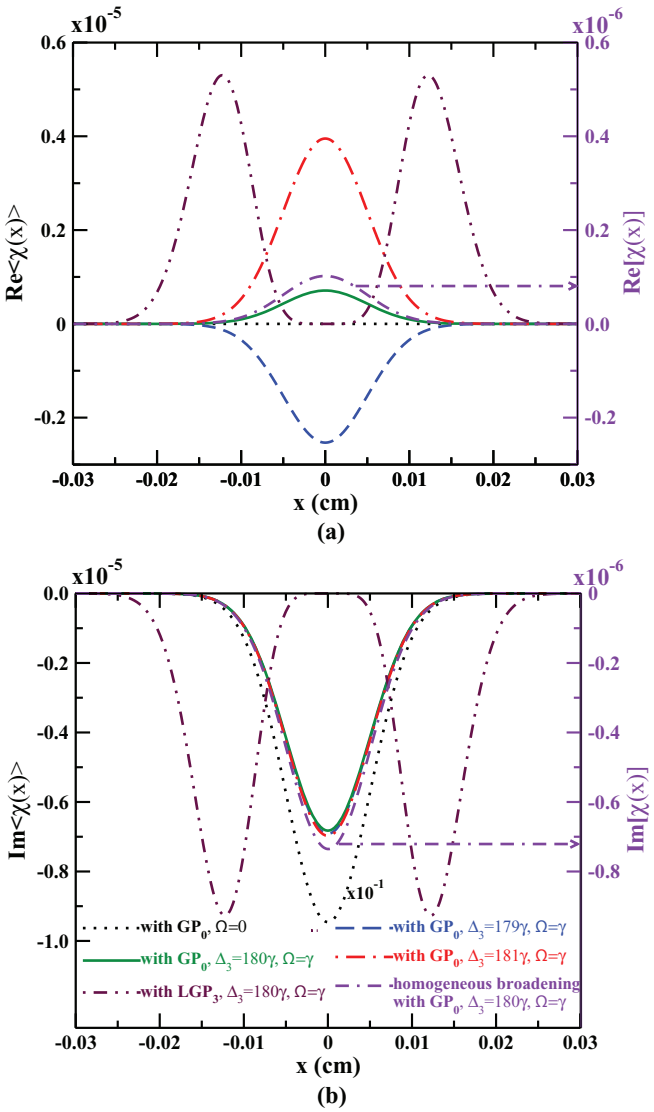

FIG. 3. (Color online) (a) Real and (b) imaginary parts of the homogeneous (right-vertical axis) and inhomogeneous (left-vertical axis) susceptibility are plotted against the transverse coordinate x at the $y = 0$ plane. The spatial probe gain profile (black dotted line) is reduced by a factor of ten to visualize it with $\Omega(x,y) = \gamma$. The Doppler width for the inhomogeneously broadened medium is $\mathcal{D} = 140\gamma$. The common parameters are fixed as follows: single-photon detuning of pump and probe fields $\Delta_1 = \Delta_2 = 180\gamma$, density $N = 2 \times 10^{10}$ atoms/cm^3, and atomic coherence decay rate $\gamma_c = 0.01\gamma$. The other parameters are the same as in Fig. 2.

like a refractive index can be mimicked in the ARG medium for $\Delta_3 \geqslant \Delta_2$. In contrast the blueshifted control field detuning $\Delta_3 < \Delta_2$ can generate a concave refractive index profile onto the medium. Therefore the refractive index gradient allows us to focus or defocus the probe beam toward the center of the pump beam. As a result the probe field propagates through the gain window with narrowing or broadening, respectively. Hence a control field can prepare a gain medium with a suitable spatial refractive index for encompassing the probe beam deflection to a great extent.

Next we consider the higher-order LGP$_3$ mode to investigate the spatial inhomogeneous character of $\langle\chi\rangle$ in the presence of a uniform control beam. The gray double-dot-dashed line in Figs. 3(a) and 3(b) shows the transverse variation of the probe refractive index as well as gain, respectively. The position dependent refractive index and gain both increase in the bright region whereas they decrease at the dark region of the doughnut shaped pump beam. In other words, LGP$_3$ induces a diverging gradient index in the region $|r| \leqslant 0.005$ cm whereas a converging gradient index exists in regions $0.005 \leqslant |r| \leqslant 0.02$ cm of the medium. Thus bright and dark regions of LGP$_3$ resemble a waveguide and antiwaveguide structure inside the atomic medium. Figure 3(a) shows that the waveguide and antiwaveguide features are accompanied with gain and absorption, respectively. As a result, the probe beam is guided out from the dark region and confined at the bright region in the course of propagation inside the medium. Hence the shape of the pump beam profile can be efficiently transferred to the transmitted probe beam.

For a homogeneously broadened medium, the violet dot-double-dashed line in Fig. 3 displays the spatial behavior of susceptibility χ in the presence of the Gaussian pump beam. We found that the features of the spatial refractive index and gain profiles of the probe field are the same as in the inhomogeneous broadened case whereas the magnitude of the susceptibilities χ are seven times smaller than the inhomogeneous case $\langle\chi\rangle$ with the same density $N = 2 \times 10^{10}$ atoms/cm^3. We thus find an important difference between inhomogeneously and homogeneously broadened atomic systems for the same atomic density. The probe beam cannot be efficiently steered at low atomic densities with a homogeneously broadened medium. However, an order-of-magnitude increase in atomic density results in efficient beam steering in the homogeneously broadened case.

B. Numerical simulation of paraxial beams equations

We have simulated numerically the propagation equations for pump [Eq. (13a)] and probe [Eq. (13b)] beams by the split step operator method [53] to demonstrate the spatial susceptibility as well as diffraction effects on the beam's propagation dynamics.

1. Optical beam steering

First, we study how the deflection of a probe beam can be controlled by a spatial dependence of the pump Rabi frequency. The shape and position of a probe beam are given by Eq. (15) at the entry face of the medium. Figure 4(a) shows the spatial evolutions of the probe beam (green solid line) with $a = 0.17$ mm and $w_p = 70\,\mu$m when the peak of the pump beam (red dashed line) is centered at the origin (0,0) with $w_c = 100\,\mu$m. Initially the overlap area between the probe and pump beam is very negligible. The overlap area is gradually increased due to the broadening of both the beams during propagation. It is evident from this figure that after a propagation of one Rayleigh length the probe beam progressively enters the pump region. The bright region of the pump beam tends to refract the probe beam into it and subsequently enhances the probe beam amplitude. As a result, the probe beam is focused toward the high intensity region of the pump and remains confined there. It is noteworthy that the probe beam gains the initial shape of the pump beam and

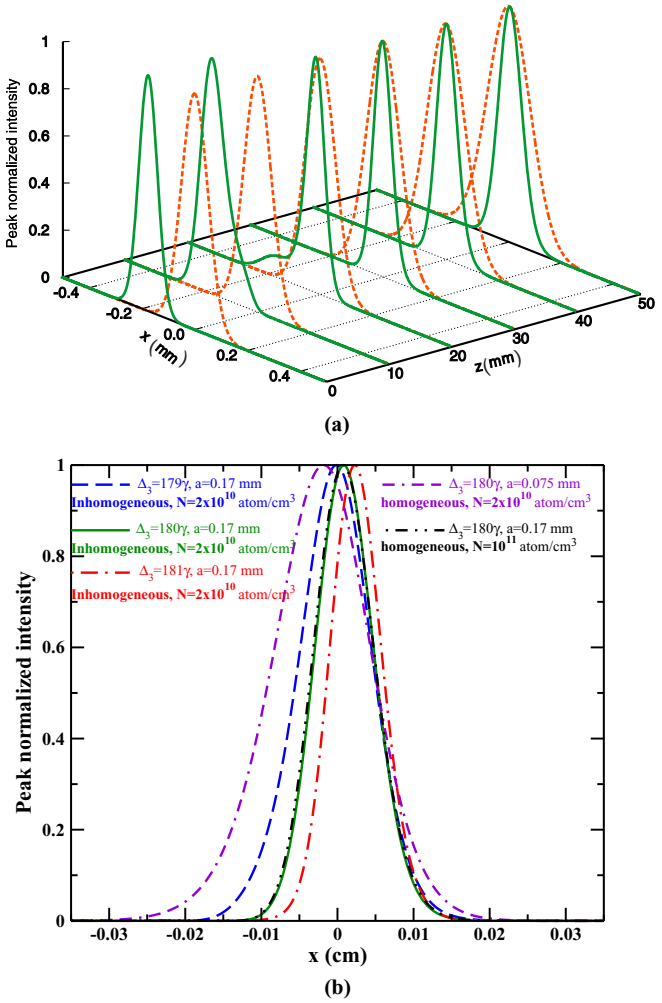

FIG. 4. (Color online) (a) The transverse probe (green solid line) and pump (red dashed line) beam intensities are plotted at different propagation distances within an inhomogeneously broadened medium. The initial amplitude, width, and initial peak location of the Gaussian probe beam are $g_0 = 10^{-3}\gamma, w_p = 70\,\mu$m, and $a = 0.17$ mm respectively. Single-photon detunings of pump, probe, and control fields are $\Delta_1 = \Delta_2 = \Delta_3 = 180\gamma$. (b) The transmitted probe beam width at a distance of 4 cm can be controllable by changing the detuning of the control field as well as densities of the atomic medium under two-photon Raman resonance condition $\Delta_1 = \Delta_2 = 180\gamma$. The initial peak positions of the probe beam are at $a = 0.075$ and 0.17 mm for a homogeneously broadened medium at two different atomic densities. The other parameters are as in Fig. 3.

retains this shape as it propagates along the z axis. Similarly, if the peak position of the probe beam is shifted along the positive x direction then it can be dragged by the pump beam toward the pump line center.

Figure 4(b) exhibits the effect of control field detuning onto the propagation dynamics of a probe pulse at $z = 4$ cm. It is seen that the deflected probe beam becomes narrower at redshifted detuning as compared to a blueshifted detuning. Therefore the sign of the detuning of the control field gives an additional flexibility to control the width of the deflected probe beam. Thus the ARG medium not only acts as an effective

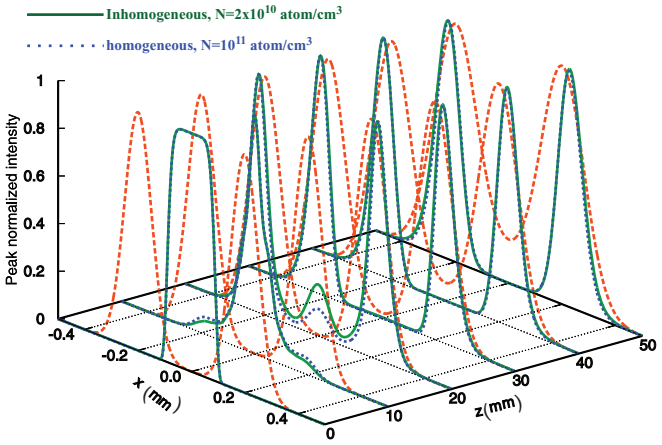

FIG. 5. (Color online) Propagation dynamics of a single super-Gaussian probe beam in the presence of a double Gaussian pump beam (red dashed line) through inhomogeneously (solid green line) as well as homogeneously (dot blue line) broadened media, respectively. The parameters are as in Fig. 4(a) except that the Gaussian probe beam is injected at center (0,0) with width $w_p = 100\,\mu$m, the double Gaussian pump beam has width 100 μm, and the atomic density for the homogeneously broadened medium is five times larger than the inhomogeneously broadened medium.

beam deflector but also can act like a lens with a wide focal length tunability.

Next we consider the propagation of the Gaussian probe beam through a homogeneously broadened medium with two different atomic densities. The initial peak position of the probe beam is at $a = 0.075$ mm for the low-density regime $N = 2 \times 10^{10}$ atoms/cm^3, whereas at high atomic density $N = 10^{11}$ atoms/cm^3 the initial peak position of the probe beam is the same as in the inhomogeneous case. Our simulation shows that the steering of the probe beam is small for the low-density regime as compared to the inhomogeneous case due to the low spatial refractive index gradient as well as low gain. The deflected probe beam suffers distortion from diffraction. However, at relatively high atomic density regime $N = 10^{11}$ atoms/cm^3, the deflection of the probe beam is the same as in the inhomogeneous broadened case. Hence the inhomogeneously broadened medium can exhibit efficient steering of the probe beam at the low-density regime as compared to the homogeneously broadened medium.

2. Optical beam splitting

Next, we demonstrate the spatial evolution of a single super-Gaussian probe as well as a double Gaussian pump beam with different propagation distance z. The solid green line and dotted blue line in Fig. 5 show the propagation dynamics through inhomogeneously and homogeneously broadened media, respectively. At the entrance face of the medium, the probe beam is launched in the dark region of the double Gaussian pump beam as shown in Fig. 5. The position dependent pump beam creates two gain peaks together with converging refractive indices in the probe susceptibility, which is similar to the gray double-dash-dotted line in Fig. 3 for both inhomogeneous and homogeneous broadened cases. The gain and spatial inhomogeneity of the refractive index are

accountable for this splitting of a single super-Gaussian probe beam into two Gaussian beams. The converging lens effect in the intense regions of the pump leads to focusing of the cloned probe beam toward it. The finesse of the transmitted probe beam can be defined as the ratio of the spacing between peaks to the width of peaks. The transmitted probe beam width is reduced by a factor of 1.5 and the peaks separations are increased by 0.7 mm as compared to the initial shape of the pump beam. Hence the finesse of the cloned image has doubly enhanced as compared with the initial pump image. Noticeably from Fig. 5 the transmitted probe beam structure is preserved even though the pump beam suffers distortion due to diffraction. Therefore, the spatial inhomogeneity of the refractive index in homogeneously as well as inhomogeneously broadened media can be used for optical beam steering.

3. Optical beam cloning

In this section, we investigate the efficient transfer of images between two copropagating orthogonal polarized optical beams. We adopt the all-optical antiwaveguide mechanism to clone the images from the pump to the probe beam. An all-optical antiwaveguide structure can be formed inside the medium with the use of the LGP_3 beam, which has zero intensity at the beam center. The dark and bright regions of the LGP_3 beam give rise to the minimum and maximum refractive index gradient on the probe susceptibility. As a result a diverging and converging refractive index are formed in the core and cladding region of the antiwaveguide structure. Thus an all-optical antiwaveguide for a probe beam is generated by the copropagating doughnut-shaped strong pump beam. In order to demonstrate the cloning mechanism in a homogeneously broadened ARG medium, the center of the dark region of the doughnut pump beam is the initial location of the probe beam. The diverging refractive index gradient and diffraction lead to the probe beam leaving the core region and slowly entering the high-intensity regions of the pump beam. Therefore each wing of the probe beam profile experiences gain and converging gradients of the refractive index in the cladding region. Thus the probe energy is guided into the annular ring of the doughnut-shaped beam and leaves a zero intensity in the dark region. Hence the transmitted probe beam profile acquires a doughnut-shaped profile as shown in Fig. 6. We have found that the transmitted structure of the probe beam is twice as sharp compared to the LGP_3 beam structure. The spatial evolution of the probe beam at different propagation distances is similar to that in Fig. 5.

4. Arbitrary image cloning

Figure 7 shows the cloning of arbitrary images and its diffraction effects through an inhomogeneously broadened ARG medium. In order to elucidate the arbitrary image cloning, we consider the probe beam as a plane wave whereas the pump beam carries a complex image such as three letters "ARG" structured at the entrance face of the medium. The two-dimensional transverse profile of the pump beam creates gain for the probe beam wherever the two-photon Raman condition is satisfied. Hence the transverse pattern of the pump beam can be efficiently transferred to the probe beam. The cloned probe beam also experiences focusing effects at the high-intensity regions of the pump beam. Thus the transmitted probe beam has better resolution than the original pump beam images as can be seen in Fig. 7(b). Figure 7(c) illustrates that the diffraction induced distortion severely affects the pump beam images and is completely distorted after a propagation of 2 cm. We also verify that the efficient transfer of arbitrary images is possible in the homogeneously broadened Raman gain medium with atomic density $N = 5 \times 10^{11}$ atoms/cm^3 [the same as shown in Fig. 7(b)].

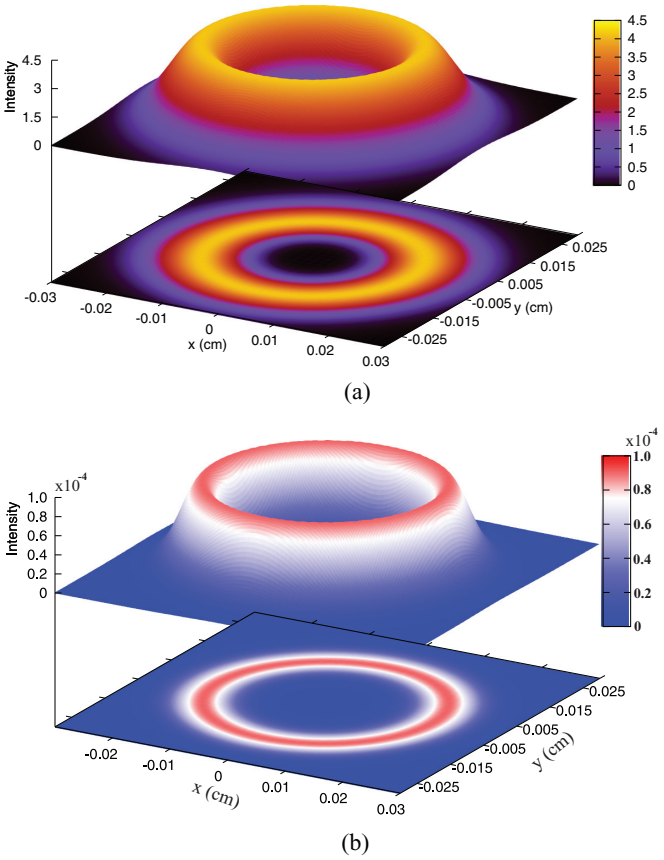

FIG. 6. (Color online) Image transfer from the doughnut-shaped pump structure to the probe beam via the antiwaveguiding mechanism. (a) The 3D intensity profile of the pump beam at the output of a 5-cm-long medium. (b) The cloned 3D probe intensity profile at the exit face of the Doppler broadened rubidium vapor cell. The other parameters are the same as in Fig. 4(a) except atomic density $N = 2 \times 10^{11}$ atoms/cm^3 and ground-state atomic coherence decay rate $\gamma_c = 0.001\gamma, G_0 = 2.5\gamma$, and $\Omega = 5\gamma$.

VI. CONCLUSION

In conclusion, we have studied diffractionless steering, splitting, and cloning of an optical beam in both a Doppler broadened as well as homogeneously broadened four-level $\mathcal{N}$-type Raman gain medium using a spatially inhomogeneous pump beam. The spatial pump beam profile gives rise to transverse modulation in the refractive index and gain for the probe beam. The modulated refractive index along with gain can optically form an antiwaveguide structure inside the medium. The properties of the antiwaveguide structure such as refractive index and gain can be controlled by the application of

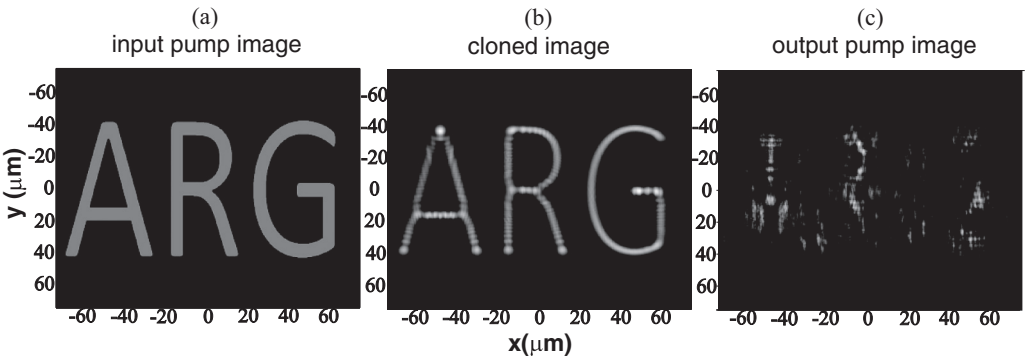

FIG. 7. (a) Three letters "ARG" are imprinted on the pump beam. (b) The efficiently transferred image onto the probe beam after 2 cm length of propagation inside the inhomogeneously broadened atomic medium. (c) The transmitted pump beam image, which is completely blurred at the exit face of the medium. The parameters are the same as in Fig. 6.

a control field, which leads to steering of the probe beam very efficiently at the low-density regime for the inhomogeneously broadened medium whereas density is relatively high for the homogeneously broadened medium. We further demonstrated that a single probe beam can be split into two Gaussian modes when it is injected at the center between two Gaussian modes of the pump beam for both inhomogeneously and homogeneously broadened media. We found that the probe beam profile has acquired the shape of the pump beam and propagates without the usual diffraction. We next show that the transfer of the doughnut-shaped pump image onto a low power Gaussian-shaped probe beam can be possible with high finesse. Finally, by numerical simulations we have established that an arbitrary image with three letters "ARG" imprinted on the pump beam can be cloned onto the transmission profile of the probe. The finesse of the cloned image has increased twice as compared to the initial resolution of pump images. Thus this scheme might be useful in optical switching, optical lithography, and optical imaging processing.

ACKNOWLEDGMENT

T.N.D. acknowledges the Science and Engineering Board of India for financial support (Grant No. SR/S2/LOP-0033/2010).

APPENDIX: EXPRESSIONS OF PROBE SUSCEPTIBILITY

The related 12th-order contributions for ρ_{32} are obtained as

$$\rho_{32}^{(12)} = \frac{i\left(\rho_{22}^{(6)} - \rho_{33}^{(6)}\right) + i\rho_{12}^{(9)} - i\Omega\rho_{34}^{(12)}}{[\gamma_{32} - i\Delta_2]}, \tag{A1}$$

$$\rho_{34}^{(12)} = \frac{i\rho_{14}^{(9)} + i\rho_{24}^{(6)} - i\Omega^*\rho_{32}^{(12)}}{[\Gamma_{34} - i(\Delta_2 - \Delta_3)]}, \tag{A2}$$

$$\rho_{12}^{(9)} = \frac{i\rho_{32}^{(3)} - i\rho_{13}^{(2)} - i\Omega\rho_{14}^{(9)}}{[\gamma_c + i\Delta_R]}, \tag{A3}$$

$$\rho_{14}^{(9)} = \frac{i\rho_{34}^{(1)} - i\Omega^*\rho_{12}^{(9)}}{[\Gamma_{41} + i(\Delta_R + \Delta_3)]}, \tag{A4}$$

$$\rho_{33}^{(6)} = \frac{i\left(\rho_{13}^{(2)} - \rho_{31}^{(1)}\right)}{[\gamma_{13} + \gamma_{23}]}, \tag{A5}$$

$$\rho_{24}^{(6)} = \rho_{44}^{(6)} = \rho_{22}^{(6)} = 0, \tag{A6}$$

$$\rho_{13}^{(2)} = \rho_{31}^{(1)} = \frac{-i}{[\Gam_{13} + i\Delta_1]}, \tag{A7}$$

$$\rho_{32}^{(3)} = \rho_{34}^{(1)} = 0, \tag{A8}$$

$$\rho_{32} = A\left[\frac{2\Gamma_{31}[\Gamma_{34} - i(\Delta_2 - \Delta_3)]}{(\gamma_{13} + \gamma_{23})\left(\Gamma_{31}^2 + \Delta_1^2\right)} + \frac{[\Gamma_{34} - i(\Delta_2 - \Delta_3)][\Gamma_{41} + i(\Delta_R + \Delta_3)] - |\Omega|^2}{(\Gamma_{31} + i\Delta_1)[(\gamma_c + i\Delta_R)[\Gamma_{41} + i(\Delta_R + \Delta_3)] + |\Omega|^2]}\right], \tag{A9}$$

with

$$A = \frac{-ig|G|^2}{(\gamma_{32} - i\Delta_2)\{\gamma_{34} - i(\Delta_2 - \Delta_3)\} + |\Omega|^2}. \tag{A10}$$

[1] I. Cindrich, Appl. Opt. **6**, 1531 (1967).
[2] D. H. McMahon, A. R. Franklin, and J. B. Thaxter, Appl. Opt. **8**, 399 (1969).
[3] W. B. Jackson, N. M. Amer, A. C. Boccara, and D. Fournier, Appl. Opt. **20**, 1333 (1981).
[4] J. D. Zook, Appl. Opt. **13**, 875 (1974).
[5] R. W. Dixon, J. Appl. Phys. **38**, 5149 (1967).
[6] G. P. Agrawal, Phys. Rev. Lett. **64**, 2487 (1990).
[7] A. T. Ryan and G. P. Agrawal, Opt. Lett. **18**, 1795 (1993).

[8] Y. Li, D. Y. Chen, L. Yang, and R. R. Alfano, Opt. Lett. **16**, 438 (1991).

[9] A. J. Stentz, M. Kauranen, J. J. Maki, G. P. Agrawal, and R. W. Boyd, Opt. Lett. **17**, 19 (1992).

[10] S. E. Harris, Phys. Today **50**, 36 (1997).

[11] M. Fleischhauer, A. Imamoglu, and J. P. Marangos, Rev. Mod. Phys. **77**, 633 (2005).

[12] E. Arimondo, Prog. Opt. **35**, 257 (1996).

[13] T. W. Hansch, M. D. Levenson, and A. L. Schawlow, Phys. Rev. Lett. **26**, 946 (1971).

[14] G. S. Agarwal and T. N. Dey, Laser and Photonics Reviews **3**, 287 (2009).

[15] O. Kocharovskaya, Phys. Rep. **219**, 175 (1992).

[16] V. A. Sautenkov, H. Li, Y. V. Rostovtsev, and M. O. Scully, Phys. Rev. A **81**, 063824 (2010).

[17] D. L. Zhou, L. Zhou, R. Q. Wang, S. Yi, and C. P. Sun, Phys. Rev. A **76**, 055801 (2007).

[18] R. Schlesser and A. Weis, Opt. Lett. **17**, 1015 (1992).

[19] R. Holzner, P. Eschle, S. Dangel, R. Richard, H. Schmid, U. Rusch, B. Rohricht, R. J. Ballagh, A. W. McCord, and W. J. Sandle, Phys. Rev. Lett. **78**, 3451 (1997).

[20] L. Karpa and M. Weitz, Nat. Phys. **2**, 332 (2006).

[21] R. R. Moseley, S. Shepherd, D. J. Fulton, B. D. Sinclair, and M. H. Dunn, Phys. Rev. Lett. **74**, 670 (1995).

[22] R. R. Moseley, S. Shepherd, D. J. Fulton, B. D. Sinclair, and M. H. Dunn, Phys. Rev. A **53**, 408 (1996).

[23] D. R. Walker, D. D. Yavuz, M. Y. Shverdin, G. Y. Yin, A. V. Sokolov, and S. E. Harris, Opt. Lett. **27**, 2094 (2002).

[24] N. A. Proite, B. E. Unks, J. T. Green, and D. D. Yavuz, Phys. Rev. A **77**, 023819 (2008).

[25] M. Mitsunaga, M. Yamashita, and H. Inoue, Phys. Rev. A **62**, 013817 (2000).

[26] A. G. Truscott, M. E. J. Friese, N. R. Heckenberg, and H. Rubinsztein-Dunlop, Phys. Rev. Lett. **82**, 1438 (1999).

[27] R. Kapoor and G. S. Agarwal, Phys. Rev. A **61**, 053818 (2000).

[28] J. A. Andersen, M. E. J. Friese, A. G. Truscott, Z. Ficek, P. D. Drummond, N. R. Heckenberg, and H. Rubinsztein-Dunlop, Phys. Rev. A **63**, 023820 (2001).

[29] M. Vengalattore and M. Prentiss, Phys. Rev. Lett. **95**, 243601 (2005).

[30] D. Bortman-Arbiv, A. D. Wilson-Gordon, and H. Friedmann, Phys. Rev. A **63**, 031801(R) (2001).

[31] G. S. Agarwal and S. Dasgupta, Phys. Rev. A **70**, 023802 (2004).

[32] C. Zhu, L. Deng, and E. W. Hagley, Phys. Rev. A **88**, 013841 (2013).

[33] G. P. Agrawal, Phys. Rev. Lett. **59**, 880 (1987).

[34] G. P. Agrawal, J. Opt. Soc. Am. B **7**, 1072 (1990).

[35] B. V. Gisin, A. A. Hardy, and B. A. Malomed, Phys. Rev. E **50**, 3274 (1994).

[36] T. N. Dey and J. Evers, Phys. Rev. A **84**, 043842 (2011).

[37] O. N. Verma and T. N. Dey, Phys. Rev. A **89**, 033830 (2014).

[38] B. E. Cohen, Nature (London) **467**, 407 (2010).

[39] E. Lantz, Nat. Photonics **2**, 71 (2008).

[40] H. Li, V. A. Sautenkov, M. M. Kash, A. V. Sokolov, G. R. Welch, Y. V. Rostovtsev, M. S. Zubairy, and M. O. Scully, Phys. Rev. A **78**, 013803 (2008).

[41] O. N. Verma, L. Zhang, J. Evers, and T. N. Dey, Phys. Rev. A **88**, 013810 (2013).

[42] D. Ding, Z. Zhou, and B. Shi, Opt. Lett. **39**, 240 (2014).

[43] M. Cao, L. Zhang, Y. Yu, F. Ye, D. Wei, W. Guo, S. Zhang, H. Gao, and F. Li, Opt. Lett. **39**, 2723 (2014).

[44] H. Wang and X. Peng, J. Opt. Soc. Am. B **29**, 429 (2012).

[45] C. Hang and V. V. Konotop, Phys. Rev. A **81**, 053849 (2010).

[46] L. Zhang and J. Evers, Phys. Rev. A **89**, 013817 (2014).

[47] M. Yan, E. G. Rickey, and Y. Zhu, Phys. Rev. A **64**, 041801(R) (2001).

[48] R. B. Li, L. Deng, and E. W. Hagley, Phys. Rev. Lett. **110**, 113902 (2013).

[49] G. Vemuri, G. S. Agarwal, and B. D. Nageswara Rao, Phys. Rev. A **53**, 2842 (1996).

[50] M. M. Kash, V. A. Sautenkov, A. S. Zibrov, L. Hollberg, G. R. Welch, M. D. Lukin, Y. Rostovtsev, E. S. Fry, and M. O. Scully, Phys. Rev. Lett. **82**, 5229 (1999).

[51] A. Javan, O. Kocharovskaya, H. Lee, and M. O. Scully, Phys. Rev. A **66**, 013805 (2002).

[52] Y. Peng, Y. Niu, L. Zhang, A. Yang, L. Jiang, and S. Gong, Opt. Lett. **37**, 3333 (2012).

[53] A. D. Bandrauk and H. Shen, J. Phys. A **27**, 7147 (1994).